

A fracture criterion for high-strength steel structural members containing notch-shape defects

J. Toribio† and F. J. Ayaso‡

*Department of Materials Engineering, University of Salamanca
E. P. S., Campus Viriato, Avda. Requejo 33, 49022 Zamora, Spain*

(Received February 15, 2002, Accepted July 24, 2003)

Abstract. This paper deals with the formulation and development of fracture criteria for high-strength structural members containing surface damage in the form of notches (i.e., blunt defects). The important role of the yield strength of the material and its strain hardening capacity (evaluated by means of the constitutive law or stress-strain curve) is analysed in depth by considering the fracture performance of notched samples taken from high-strength steels with different levels of cold drawing (the most heavily drawn steel being commercial prestressing steel used in prestressed concrete). The final aim of the paper is to establish fracture-based design criteria for structural members made of steels with distinct yield strength and containing very different kinds of notch-shape surface damage.

Key words: fracture criterion; high-strength steel; cold drawn wires; notched structural members; structural engineering.

1. Introduction

The study of high-strength prestressing steels has special importance in civil engineering structures where prestressed concrete is widely used. These steels are manufactured from a previously hot rolled bar with pearlitic microstructure which is heavily cold drawn in several passes to produce the commercial prestressing steel wire with increased yield strength obtained by a mechanism of strain-hardening. Then the final commercial product has undergone strong plastic deformations able to modify its microstructure. Thus, although cold drawing improves the (traditional) mechanical properties of the steel (i.e., those properties useful for regular service), the microstructural changes during manufacture may affect the fracture performance of the material, specially in the presence of stress raisers like cracks or notches (Elices 1985, Hancock and Mackenzie 1976, Mackenzie *et al.* 1977, Hancock and Brown 1983).

In addition, notch-like defects (i.e., with root radius different from zero) are very frequent in structural components (Elices 1985) due to the particular working conditions (e.g. anchorages for prestressed concrete). They generate a triaxial stress distribution near the notch (cf. cracked ones), which allows a detailed analysis of the influence of stress state and triaxiality on ductile failure (Boonchukosol and Gasc 1979, Beremin 1980) and microscopic mechanisms of fracture (Thompson 1985, Alexander and Bernstein 1982).

†Professor

‡Doctor

The final aim of this paper is the analysis of the fracture process in high strength pearlitic steel governed by two key variables: the *stress triaxiality* in the vicinity of the notch tip (produced by notches of very different depths and radii) and the *yield strength* of the material (controlled by the degree of cold drawing achieved during the manufacturing process to make prestressing steel for civil engineering).

2. Experimental programme

Samples from a real manufacturing process were supplied by EMESA TREFILERIA. The manufacture chain was stopped in the course of the process, and samples of five intermediate stages were extracted, apart from the original material or base product (hot rolled bar: not cold drawn at all) and the final commercial product (prestressing steel wire: heavily cold drawn). Thus the *drawing intensity* (or straining level) is treated as the fundamental variable to elucidate the consequences of manufacturing on the posterior fracture behaviour.

The different steels were named with digits 0 to 6 which indicate the number of cold drawing steps undergone. Table 1 shows the chemical composition common to all steels, and Table 2 includes the diameter (D_i), the cold drawing degree (D_i/D_0), the yield strength (σ_{02}), the ultimate tensile stress (UTS) and the fracture toughness (K_{IC}) of the steels.

The stress-strain curves of the seven steels with increasing degree of cold drawing appear in Fig. 1, where a clear improvement of traditional mechanical properties is achieved after manufacturing, due to a strain hardening mechanism activated in the steels. The manufacturing process by cold drawing also produces an induced texture and anisotropic fracture behaviour of the different steels, as analysed in detail in a previous paper (Toribio and Ayaso 2003).

The curves of steels A2 to A5 are terminated at a strain about 2% because the maximum load in the standard tensile test appeared at such a strain, probably because the surface finishing of those steels (with *intermediate* degree of cold drawing) had lower quality due to characteristics of the industrial manufacturing chain that was stopped to obtain the different materials. However, this fact does not affect the analysis presented in this paper, since the stress-strain path of the intermediate steels (A2 to A5) is clearly defined by the curves shown in Fig. 1, which allows a characterization of the stress-strain trajectory for each steel. In addition to this, Fig. 1 undoubtedly shows that the curves of steels A2 to A5

Table 1 Chemical composition of the steels

C	Mn	Si	P	S	Cr	V	Al
0.80	0.69	0.23	0.012	0.009	0.265	0.060	0.004

Table 2 Diameter (D_i), cold drawing degree (D_i/D_0), yield strength (σ_{02}), ultimate tensile stress (UTS) and fracture toughness (K_{IC}) of the different steel wires

Steel	0	1	2	3	4	5	6
D_i (mm)	12.00	10.80	9.75	8.90	8.15	7.50	7.00
D_i/D_0	1	0.90	0.81	0.74	0.68	0.62	0.58
σ_{02} (GPa)	0.686	1.100	1.157	1.212	1.239	1.271	1.506
UTS(GPa)	1.175	1.294	1.347	1.509	1.521	1.526	1.762
K_{IC} (MPam ^{1/2})	60.1	61.2	70.0	74.4	110.1	106.5	107.9

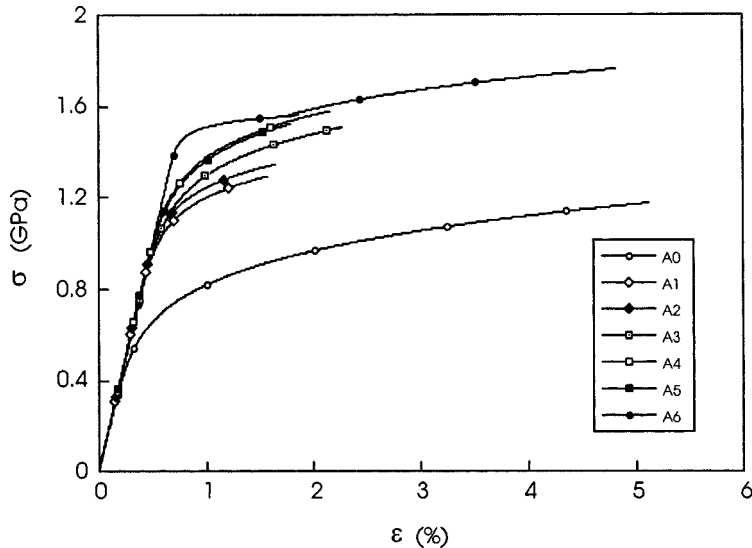


Fig. 1 Stress-strain curves of the different steels used in the experimental programme

present similar appearance to that of steel A0, and thus, although the former are really shorter due to experimental instabilities, they give enough information to define the stress-strain path of these intermediate steels on the basis of the more prolonged curve of steel A0 (steel A6 is special because it has suffered a final thermomechanical treatment to eliminate residual stresses in the final commercial product and thus it exhibits a different shape in the σ - ε curve). Furthermore, the validity of the afore-said reasoning will again be emphasized by the excellent agreement between the experimental load-displacement plots and the numerically predicted ones (using the curves of Fig. 1), as shown in further sections of this paper.

Fracture tests under tension loading were performed on axisymmetric notched specimens with a circumferentially-shaped notch. Four notch geometries were used with each material, in order to achieve very different stress states in the vicinity of the notch tip and thus very distinct *constraint* situations, thus allowing an analysis of the influence of such factors on the fracture processes. The dimensions of the specimens - named A, B, C and D throughout this paper - were the following:

- Geometry A : $R/D = 0.03$, $C/D = 0.10$
- Geometry B : $R/D = 0.05$, $C/D = 0.30$
- Geometry C : $R/D = 0.40$, $C/D = 0.10$
- Geometry D : $R/D = 0.40$, $C/D = 0.30$

where R is the notch radius, C the notch depth and D the external diameter of the specimen. These four notched geometries are depicted in Fig. 2.

Three fracture tests were performed for each material and geometry (thus a total number of 84 tests were performed: seven materials, four notched geometries and three tests of each) under displacement control and recording continuously the load and the relative displacement between two points distant 25 mm (the gage length of the extensometer).

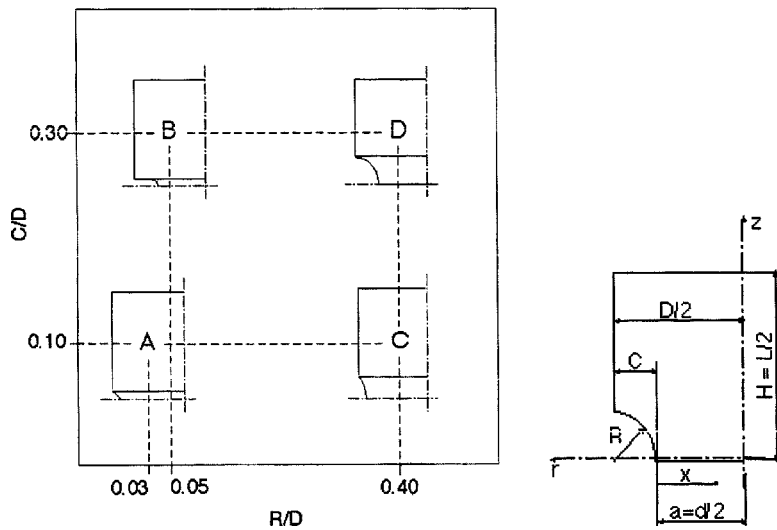


Fig. 2 Notched geometries used in the experimental programme

3. Experimental results

The experimental results of the tests performed with the four notched samples of the seven steels are given in Figs. 3, 4, 5 and 6 in the form of load vs. displacement for the representative test of each group of three (that displaying the intermediate curve). In the test name, the first digit indicates the steel, and the second represents the notch geometry of the specimen.

No significant differences between the analysed steels are observed in the matter of the shape of the F-u curves. Such a shape is dependent *only* of the notch geometry, i.e., of the *stress triaxiality* (or *constraint*), whereas the size of the curves (maximum load level) does depend on the steel in particular.

Geometries A and B (sharply notch specimens) present a macroscopically brittle fracture behaviour with failure at the point of maximum load in the load-displacement plot (cf. Figs. 3 and 4) and an abrupt decrease of load up to the zero level, which produces a sudden interruption of the load-displacement path under displacement control, a typical experimental output (sudden failure with abrupt load drop) associated with brittle fracture behaviour (Landes 1994). On the other hand, in geometries C and D (bluntly notched specimens) the fracture behaviour is ductile, associated with a detectable decrease in load in the F-u curves as the displacement increases (Landes 1994). The described brittle or ductile behaviour is consistent with the fractographic analysis performed on the samples after the tests (cf. Toribio and Ayaso 2002), showing that geometries A and B (macroscopically brittle fracture behaviour) exhibit fracture initiation at the notch tip with fast propagation by cleavage (microscopically brittle fracture mode), whereas geometries C and D (macroscopically ductile fracture behaviour) exhibit fracture initiation in a extended area in the specimen centre in which the fracture process develops slowly by micro-void coalescence (microscopically ductile fracture mode), in the same manner as the cup and cone fracture after necking (decreasing part of the load-displacement plot) in a standard tension test.

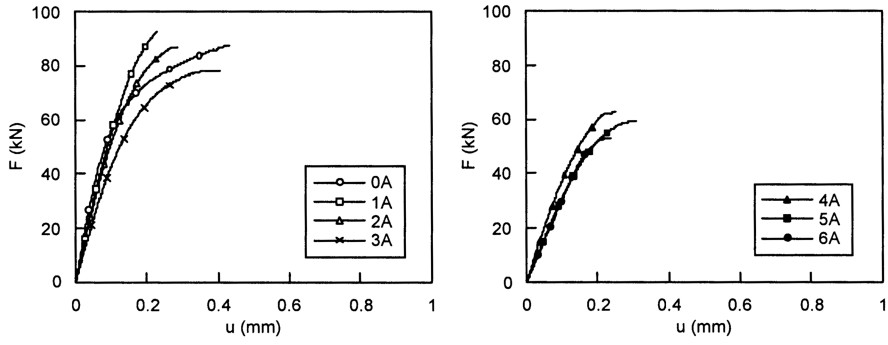


Fig. 3 Load-displacement curves (sample A)

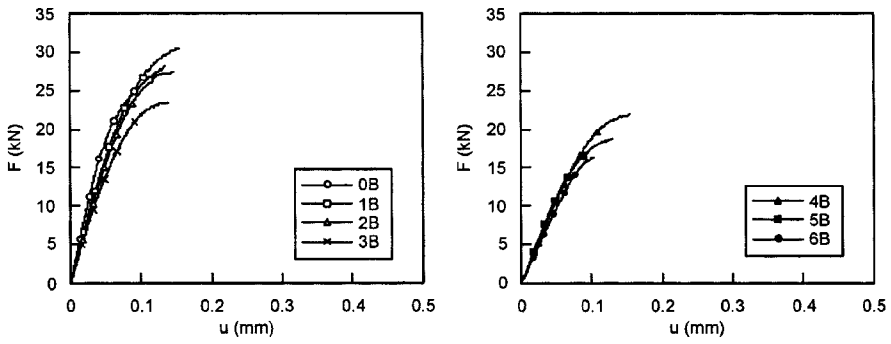


Fig. 4 Load-displacement curves (sample B)

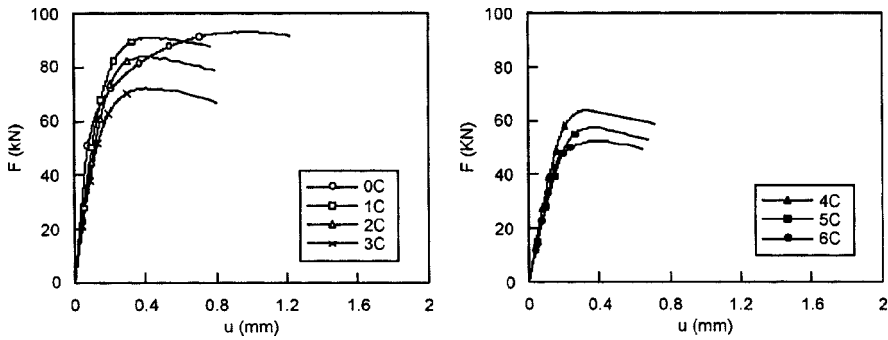


Fig. 5 Load-displacement curves (sample C)

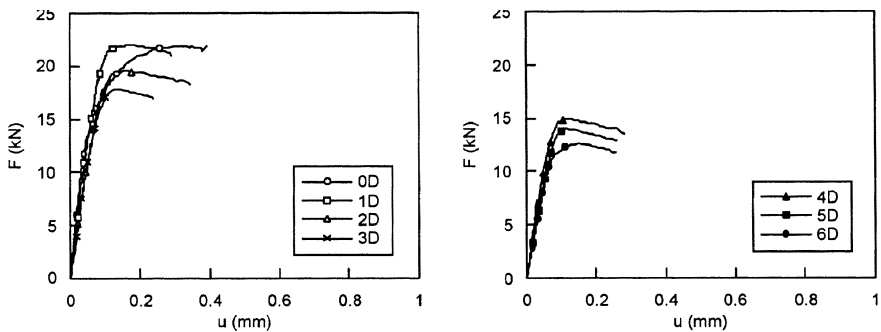


Fig. 6 Load-displacement curves (sample D)

4. Numerical modelling

In a fracture test the macroscopic external variables (force, displacement, ...) can be measured and the microscopic modes of fracture observed by scanning electron microscopy. To find the distribution of macroscopic internal variables in the continuum mechanics sense (stress, strain, strain energy density, ...) at any time, and particularly at the moment of fracture, the elastic-plastic finite element method (FEM) was applied, using a Von Mises yield surface.

The external load was applied step by step, in the form of nodal displacements. An improved Newton-Raphson method was adopted, which modified the tangent stiffness matrix at each step. Large strains and large geometry changes were used in the computations by means of an updated lagrangian formulation, so as to predict the evolution of mechanical variables in the samples after the instant of maximum load (i.e., after the point of instability under load control), up to the instant of final failure by physical separation of the two fracture surfaces (i.e., up to the point of instability under displacement control).

The constitutive equation of the material - as a relationship between equivalent stress and strain- was introduced into the computer program from the real experimental results of the standard tension tests in the considered materials (see Fig. 1). The curves were extended for large strains on the basis of the volume conservation in classical Plasticity and accounting for the strain hardening evolution to obtain steel 6 from the previous materials (steels 0 to 5).

The finite elements used in the computations were isoparametric with second-order interpolation (eight -node quadrilaterals and six-node triangles). The problem presents double symmetry, so as only a quarter of the sample has to be analysed, and the displacements were fixed along the axes of symmetry (boundary conditions).

Fig. 7 shows the four finite element meshes used in the computations associated with steel 0 and notched geometries A, B, C and D. The meshes used with steels 1 to 6 are similar to these, i.e., they have the same distribution of elements (the same topology as those used with steel 0) but their dimensions are proportional to the wire diameter in each particular case.

Figs. 8 and 9 offer a comparison of the load-displacement curves really obtained in the fracture experiments and those numerically predicted by using the finite element method. Results for all geometries (A, B, C, D) and steel 0 (Fig. 8) and steel 6 (Fig. 9) are plotted. The agreement can be considered as excellent in all cases, which indicates that the numerical modelling is accurate enough to

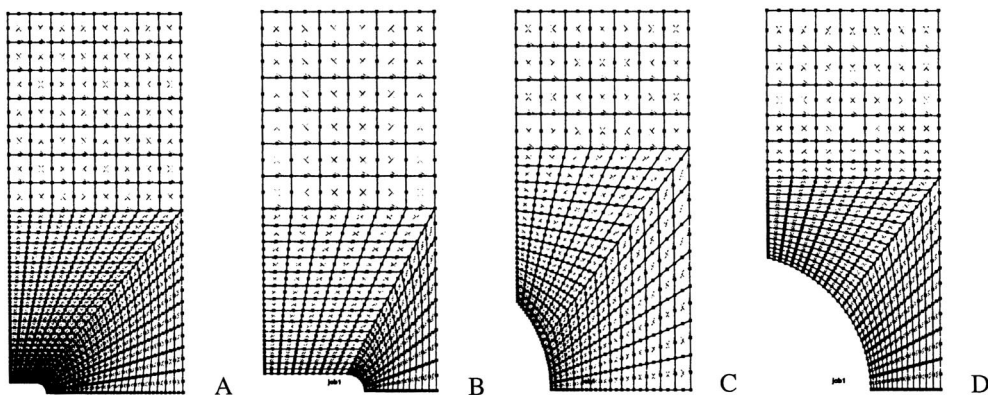


Fig. 7 Finite element meshes used in the numerical computations. Those for steel 0 and geometries A, B, C and D are shown. Meshes for steels 1 to 6 are similar

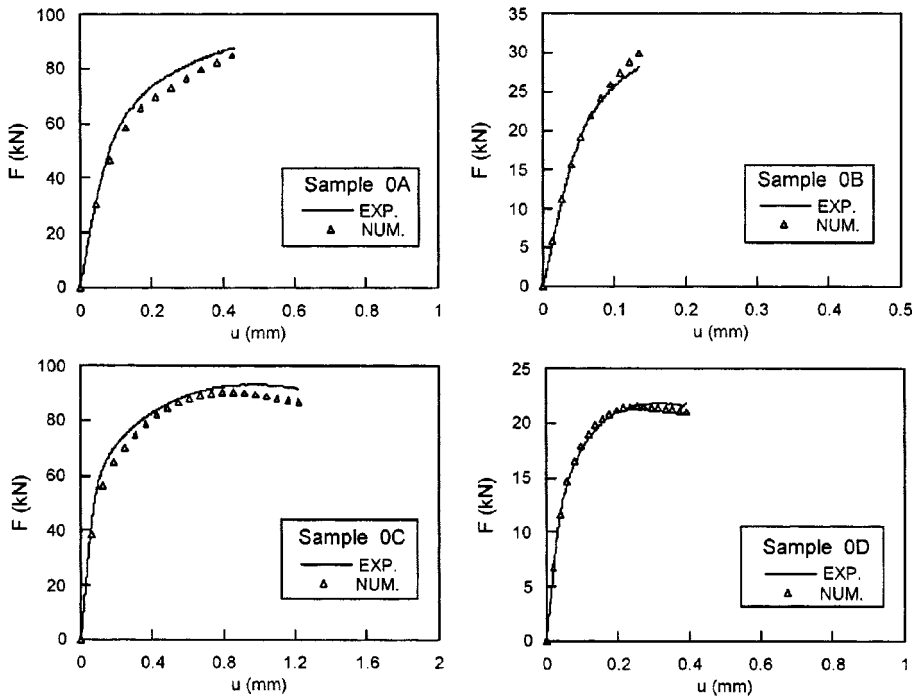


Fig. 8 Experimental results (EXP) and numerical predictions (NUM) for steel 0

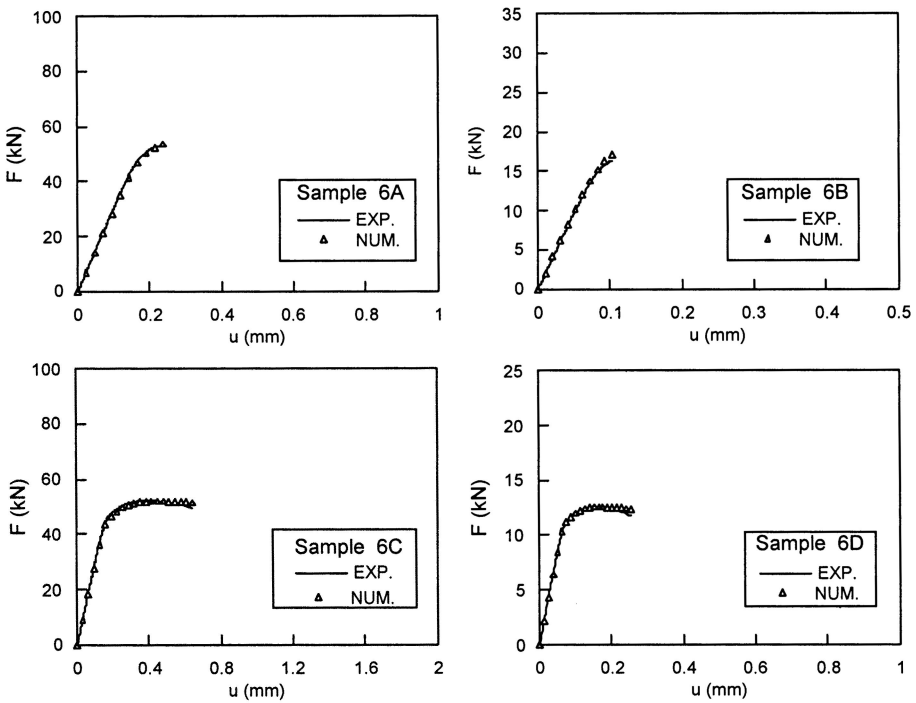


Fig. 9 Experimental results (EXP) and numerical predictions (NUM) for steel 6

predict the evolution of internal (continuum mechanics variables) in the specimens up to the final fracture moment of instability under displacement control, the numerical prediction of the load decrease part of the curve being also very good. This fact again demonstrates the goodness of the stress-strain trajectories used for each steel in the computations, on the basis of the σ - ϵ curves shown in Fig. 1.

5. Failure analysis

The numerical finite element method allows the computation of internal variables (in the continuum mechanics sense) at any instant, and particularly at the moment of failure.

The analysed variables were the following:

- The hydrostatic stress, or mean normal stress, defined as one third of the trace of the stress tensor.
- The effective or equivalent stress defined in the Von Mises sense of the mathematical theory of plasticity.
- The stress triaxiality, defined as the ratio of the hydrostatic stress to the effective or equivalent stress.
- The axial stress, i.e., the component of the stress tensor which is parallel to the main loading axis.
- The equivalent plastic strain as a measure of accumulated mechanical damage in the notched samples.
- The strain energy density, together with its elastic and plastic components, as well as the dilatational and the distortional ones.

Figs. 10 and 11 show the distributions of hydrostatic and equivalent stresses, as well as triaxiality at the failure situation (instability point under displacement control) for steel 0 (hot rolled material which is not cold drawn) and steel 6 (commercial prestressing steel wire which is heavily drawn).

The hydrostatic stress reaches its maximum at a small distance from the notch tip in geometries A and B (those of minimum notch radius), and at the specimen axis in geometries C and D (those of maximum notch radius). In the latter case of notched specimens C and D there is a displacement of such a maximum hydrostatic stress point from the vicinity of the notch tip (at the early steps of the loading process) to the axis of the specimen at the latter steps of the loading process, including the load decrease part of the load-displacement curve after the instability point under load control (point of maximum). This numerical result could have a crucial influence in environmentally assisted fracture processes in hydrogen embrittlement conditions, because hydrogen is driven by the hydrostatic stress field towards the locations of maximum hydrostatic stress (Toribio and Elices 1992)

The equivalent stress in the Von Mises sense reaches its maximum value at the notch tip in geometries A y B (lower notch radius) and it follows a quasi-constant radial distribution in geometries C and D (higher notch radius). In the former case there is a sudden decrease after the maximum as the distance x (from the notch tip) increases.

In the matter of triaxiality, the conclusions are similar to those drawn for the hydrostatic stress in geometries A, C and D. The only exception is the distribution of triaxiality in geometry B (that with the highest levels of constraint) in which, although the hydrostatic stress is maximum near the notch tip, the triaxiality reaches its maximum at a deeper point nearer to the specimen axis, it being exactly located at that axis in the steel 6.

With regard to the influence of the constitutive equation of the material (which can be analysed through the stress-strain curve), it is seen that the corresponding plots of Figs. 10 and 11 are really similar, which means that the influence of the stress-strain curve of each material is of minor influence on the distribution of the main internal variables (hydrostatic and equivalent stresses and triaxiality).

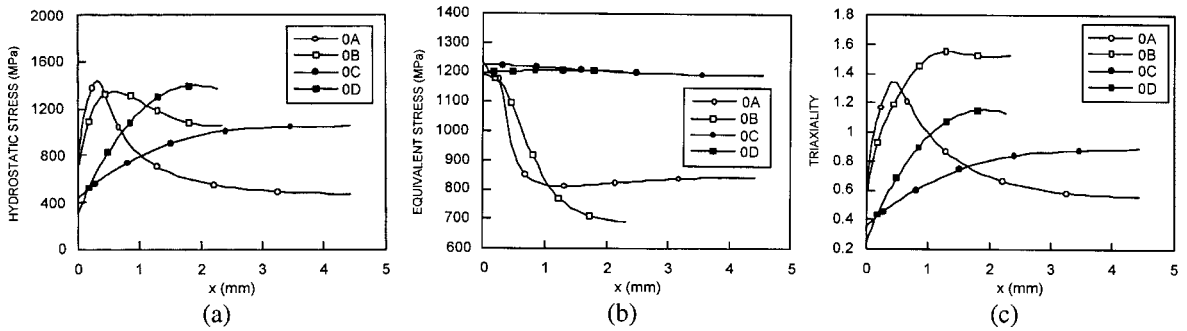


Fig. 10 Distributions of hydrostatic stress (a) equivalent stresses (b) and stress triaxiality (c) at the final failure situation or instability point under displacement control for steel 0 (hot rolled material which is not cold drawn) and notched geometries A, B, C and D. In the horizontal axis the coordinate x represents the radial distance measured from the notch tip (thus $x=0$ is the tip itself and the specimen axis is located at the right hand side)

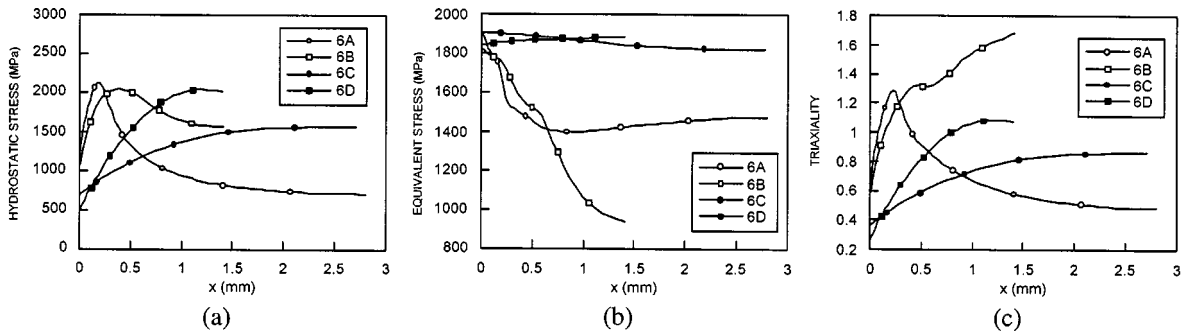


Fig. 11 Distributions of hydrostatic stress (a) equivalent stresses (b) and stress triaxiality (c) at the final failure situation or instability point under displacement control for steel 6 (cold drawn wire or prestressing steel) and notched geometries A, B, C and D. In the horizontal axis the coordinate x represents the radial distance measured from the notch tip (thus $x=0$ is the tip itself and the specimen axis is located at the right hand side)

The only exception is again the distribution of triaxiality in geometry B in which the rising slope of the triaxiality law (for increasing coordinate x) is quite higher in steel 6 than in steel 0.

Fig. 12 plots the distributions of axial stress, equivalent plastic strain and total strain energy density (SED). The first represents the component of the stress tensor in the loading direction and could influence purely brittle fracture processes; the second is a measure of mechanical pre-damage in the samples and the third has a clear energetic meaning which could influence the fracture process.

In geometries A and B (those of minimum notch radius) the maxima are achieved in the vicinity of the notch tip (axial stress) and exactly at the notch tip (equivalent plastic strain and strain energy density). Geometry C exhibits the maximum axial stress at the specimen axis and the maxima of both the equivalent plastic strain and the strain energy density near the notch tip. In geometry D the three maxima of axial stress, equivalent plastic strain and strain energy density are achieved just at the specimen axis, the slope of the distribution being higher in the case of the axial stress.

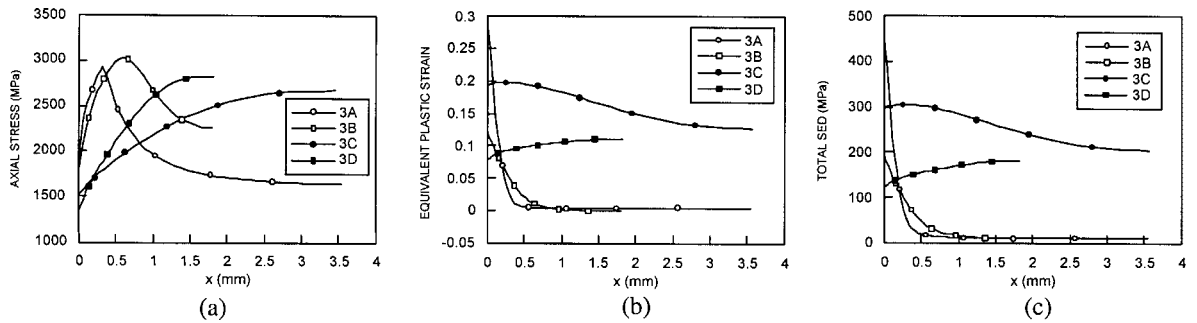


Fig. 12 Distributions of axial stress (a) equivalent plastic strain (b) and total strain energy density (c) at the final failure situation or instability point under displacement control for steel 3 (with an intermediate degree of cold drawing) and notched geometries A, B, C and D. In the horizontal axis the coordinate x represents the radial distance measured from the notch tip (thus $x=0$ is the tip itself and the specimen axis is located at the right hand side)

6. Formulation of a fracture criterion

The formulation of the failure criterion for the notched specimens of high strength pearlitic steels with different degrees of cold drawing is based on the question whether or not there is a governing variable (in the sense of continuum mechanics) which reaches a critical value at the fracture initiation point (space localisation) and at the failure instant (time localisation), that critical value being independent of the specimen geometry and thus dependent only of the material (a material characteristic value):

Then the failure criterion could be formulated in general terms as follows:

Failure will take place when the proper governing variable (in the continuum mechanics sense) reaches a critical value at the fracture initiation point.

With regard to the space localisation, the search of the initiation point is made on the basis of a very detailed fractographic analysis (cf. Ayaso 2001) after which it is seen that failure initiates at the notch tip in specimens A and B (notched geometries of minimum radius) and at the sample axis in specimens C and D (notched geometries of maximum radius).

In the matter of time localisation, the failure situation considered in this paper is that associated with the final fracture by physical separation of the fracture surfaces, i.e., the point of instability under displacement control in the load-displacement plots. In the case of geometries A and B, such a point coincides with the point of instability under load control, since in those specimens there is no load decrease in the load-displacement plots.

Now the objective is to find the governing variable at the failure situation. To this end, the distributions of internal variables (in the continuum mechanics sense) plotted in Figs. 10 to 12 should be analysed to find out which of them reaches a characteristic value at the notch tip in geometries A and B and at the specimen axis in geometries C and D. The only candidate is the effective or equivalent stress in the Von Mises sense.

To check the real adequacy of this equivalent stress as the internal variable governing the failure

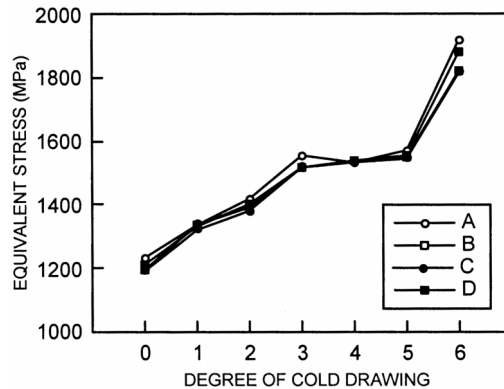


Fig. 13 Effective or equivalent stress at the failure situation in notched samples A, B, C and D of steels with variable degree of cold drawing (represented in the horizontal axis by the number of cold drawing steps undergone by each steel)

situation with independence of the notch geometry, Fig. 13 shows a plot representing such a stress in the different notched geometries (A, B, C and D) *versus* the degree of cold drawing (number of drawing steps undergone by each steel).

It is seen that the Von Mises equivalent stress reaches a characteristic value in each step with independence of the notch geometry and thus the failure process is governed by such a variable with physical meaning, since it is one-to-one related to the distortional part of the strain energy density.

Finally the failure criterion may be formulated in specific terms as follows:

Failure will take place when the distortional part of the strain energy density (or, accordingly, the effective or equivalent stress in the Von Mises sense) reaches a critical value at the fracture initiation point.

where the fracture initiation point is the notch tip in those geometries of minimum tip radius and the specimen axis in those geometries of maximum tip radius. The choice of a single point to apply the failure criterion is equivalent to the assumption of a characteristic distance (related to the microstructure of the material) very small: of the order of one or two times the size of one of the characteristic microstructural levels: the pearlite colony size or the pearlitic interlamellar spacing. Those sizes vary as a function of the degree of cold drawing, the pearlite colony size ranging between 5 and 15 μm and the pearlitic interlamellar spacing ranging between 0.03 and 0.06 μm , after the measurement performed previously (Ovejero 1998).

7. Conclusions

A failure analysis of high-strength structural members containing notch-shape defects with very different geometries (very distinct notch depths and radii) was presented in this paper, on the basis of a broad experimental program of fracture tests on notched specimens and posterior numerical analysis by the finite element method.

From the experimental view point, it was seen that specimens A and B (those of minimum notch radius) fail in a brittle manner with no load decrease in the load-displacement curve. On the other hand,

specimens C and D (those of maximum notch radius) fail in a ductile manner associated with load-decrease in the load-displacement curve.

The numerical results show that the main internal variables reach their maximum values at the notch tip or in its vicinity in the case of specimens A and B and at the sample axis in the case of specimens C and D, which is consistent with the fractographic analysis and with the previous conclusion about the brittle behaviour of the former and the ductile behaviour of the latter.

A failure criterion was formulated for notched samples of high-strength pearlitic steel with different degrees of cold drawing: failure will take place when the distortional part of the strain energy density (or, accordingly, the effective or equivalent stress in the Von Mises sense) reaches a critical value at a small region characteristic of the material microstructure.

Acknowledgments

Financial support (Grant MAT2002-01831) of this work by the Spanish Ministry of Science and Technology (MCYT) and FEDER is gratefully acknowledged. In addition, the authors wish to express their gratitude to EMESA TREFILERIA S.A. (La Coruña, Spain) for providing the steel used in the experimental programme.

References

- Alexander, D.J. and Bernstein, I.M. (1982), "The cleavage plane of pearlite", *Metall. Trans.*, **13A**, 1865-1868.
- Ayaso, F.J. (2001), "Fractura de alambres entallados de acero progresivamente trefilado", Ph. D. Thesis, University of La Coruña, Spain.
- Beremin, F.M. (1980), "Influence de la triaxialité des contraintes sur la rupture par déchirement ductile et la rupture fragile par clivage d'un acier doux", *Journal de Mécanique Appliquée*, **4**, 327-342.
- Boonchukosol, K. and Gasc, C. (1979), "Influence de l'état de contrainte sur les conditions de rupture des aciers", *Journal de Mécanique Appliquée*, **3**, 105-118.
- Elices, M. (1985), "Fracture of steels for reinforcing and prestressing concrete", in *Fracture Mechanics of Concrete* (Eds., Sih, G.C. and DiTommaso, A.), pp. 226-271. Martinus Nijhoff Publishers, Dordrecht, The Netherlands.
- Hancock, J.W. and Brown, D.K. (1983), "On the role of strain and stress state in ductile failure", *J. Mech. Phys. Solids*, **31**, 1-24.
- Hancock, J.W. and Mackenzie, A.C. (1976), "On the mechanisms of ductile failure in high-strength steels subjected to multi-axial stress-states", *J. Mech. Phys. Solids*, **24**, 147-169.
- Landes, J.D. (1994), "The effect of constraint on fracture safe design", in *Structural Integrity: Experiments, Models, Applications / ECF 10* (Eds. K. H. Schwalbe and C. Berger), pp. 23-35. EMAS, West Midlands, UK.
- Mackenzie, A.C, Hancock, J.W. and Brown, D.K. (1977), "On the influence of state of stress on ductile failure initiation in high strength steels", *Engng. Fracture Mech.*, **9**, 167-188 (1977).
- Ovejero, E. (1998), "Fractura en ambiente agresivo de aceros perlíticos con distinto grado de trefilado", Ph. D. Thesis, University of La Coruña, Spain.
- Thompson, A.W. (1985), "Hydrogen assisted fracture at notches", *Mater. Sci. Tech.*, **1**, 711- 718.
- Toribio, J. and Ayaso, F. J. (2002), "Fracture process zone in notched samples of cold drawn pearlitic steels", *ISIJ International* **42**, 1049-1055.
- Toribio, J. and Ayaso, F. J. (2003), "Anisotropic fracture behaviour of cold drawn steel: a materials science approach", *Mater. Sci. Engng.* **A343**, 265-272.
- Toribio, J. and Elices, M. (1992), "The role of local strain rate in the hydrogen embrittlement of round notched samples", *Corros. Sci.*, **33**, 1387-1409.